LAWRENCE
LIVERMORE
NATIONAL
LABORATORY

UCRL-JRNL-237225

NIMROD Resistive Magnetohydrodynamic Simulations of Spheromak Physics

E. B. Hooper, B. I. Cohen, H. S. McLean, R. D. Wood, C. A. Romero-Talamas, C. R. Sovinec

December 12, 2007

Physics of Plasmas

Disclaimer

NIMROD resistive magnetohydrodynamic simulations of spheromak physics

E. B. Hooper,[a,b] B. I. Cohen,[a,c] H. S. McLean, R. D. Wood, and C. A. Romero-Talamas

University of California Lawrence Livermore National Laboratory

P.O. Box 808

Livermore, CA 94550

C.R. Sovinec

Department of Engineering Physics

University of Wisconsin-Madison, Madison, WI 53706-1609

Abstract

The physics of spheromak plasmas is addressed by time-dependent, three-dimensional, resistive magneto-hydrodynamic simulations with the NIMROD code. Included in some detail are the formation of a spheromak driven electrostatically by a coaxial plasma gun with a flux-conserver geometry and power systems that accurately model the Sustained Spheromak Physics Experiment (SSPX) (R. D. Wood, et al., Nucl. Fusion **45**, 1582 (2005)). The controlled decay of the spheromak plasma over several milliseconds is also modeled as the programmable current and voltage relax, resulting in simulations of entire experimental pulses. Reconnection phenomena and the effects of current profile evolution on the growth of symmetry-breaking toroidal modes are diagnosed; these in turn affect the quality of magnetic surfaces and the energy confinement. The sensitivity

of the simulation results address variations in both physical and numerical parameters, including spatial resolution. There are significant points of agreement between the simulations and the observed experimental behavior, *e.g.*, in the evolution of the magnetics and the sensitivity of the energy confinement to the presence of symmetry-breaking magnetic fluctuations.

[a)]These two authors contributed equally to this paper.

[b)]Electronic mail: hooper1@llnl.gov

[c)]Electronic mail: cohen1@llnl.gov

I. INTRODUCTION

Spheromak plasmas are an interesting alternative confinement concept as compared to tokamaks. Spheromaks are typically more compact, have no center conductor, and operate at higher ratios of plasma pressure to magnetic pressure; and the investment in the confining magnetic structure and coils is more modest. These features in aggregate potentially make a spheromak power reactor more attractive than a tokamak reactor if the spheromak plasma can exhibit as much stability and favorable energy confinement. Electron temperatures T_e near 400 eV were observed transiently in the Los Alamos Compact Torus Experiment (CTX) spheromak experiment,[1] and higher temperatures have been observed to persist in the SSPX spheromak as long as proper discharge conditions are maintained.[2,3] Understanding the formation and decay of spheromaks and the energy confinement therein is a challenging problem. Results from numerical simulations with the NIMROD nonlinear resistive MHD code (at zero or finite plasma pressure) have shown that closed flux surfaces with net current can arise only after electrostatic drive is reduced.[4,5] Other calculations with NIMROD have directly investigated the importance of inductive effects on energy confinement including the evolution of the temperature and number density using thermal transport coefficients, electrical resistivity, and Ohmic heating. These simulations have elucidated the role of the current-profile evolution in influencing the growth of symmetry-breaking modes, which in turn affect the quality of the magnetic surfaces and the energy confinement.[5,6,7] NIMROD simulations have also demonstrated the intimate relationship between inductive effects, magnetic reconnection and build-up of the magnetic field.[8] The magneto-hydrodynamic (MHD) model combined with collisional transport is a

reasonable approximation because the collisional mean-free path is less than the axisymmetric flux-conserver radius R=0.5m for nominal SSPX plasma parameters on open magnetic field lines with n~5×10^{19} m^{-3}, T≤35 eV, and singly charged ions.

The simulations are performed with the NIMROD three-dimensional, resistive MHD code.[4,9] The simulations solve nonlinear time-dependent equations for particle number density (n_i=n_e=n with quasineutrality), plasma flow velocity (**V**), temperature (assuming T_i=T_e=T), and magnetic field (**B**). In MKS units, the evolution equations are

$$\frac{\partial n}{\partial t} + \nabla \cdot \left(n\mathbf{V} \right) = \nabla \cdot D\nabla n \tag{1}$$

$$\rho \left(\frac{\partial \mathbf{V}}{\partial t} + \mathbf{V} \cdot \nabla \mathbf{V} \right) = \mathbf{J} \times \mathbf{B} - \nabla p + \nabla \cdot \rho \nu \nabla \mathbf{V} \tag{2}$$

$$\frac{nk_B}{\gamma - 1} \left(\frac{\partial T}{\partial t} + \mathbf{V} \cdot \nabla T \right) = -\frac{p}{2} \nabla \cdot \mathbf{V} + \nabla \cdot nk_B \left[\chi_{\parallel} \hat{\mathbf{b}}\hat{\mathbf{b}} + \chi_{\perp} \left(\mathbf{I} - \hat{\mathbf{b}}\hat{\mathbf{b}} \right) \right] \cdot \nabla T + \frac{\eta \mathbf{J}^2}{2} \tag{3}$$

$$\frac{\partial \mathbf{B}}{\partial t} = \nabla \times \left(\mathbf{V} \times \mathbf{B} - \eta \mathbf{J} \right) \tag{4}$$

$$\mu_0 \mathbf{J} = \nabla \times \mathbf{B} \tag{5}$$

where $p \equiv 2nk_BT$ is the sum of electron and ion pressures, and $\hat{\mathbf{b}} \equiv \mathbf{B}/|\mathbf{B}|$ is the evolving magnetic direction vector field. The simulations consider n, T, **V**, **B**, and **J** to be functions of all three spatial dimensions and time. Thus, induction of the spheromak equilibrium from magnetic fluctuations and energy transport from heat-flow fluctuations are modeled explicitly. The boundary conditions are $\mathbf{E} \times \hat{\mathbf{n}} = \delta\mathbf{B} \cdot \hat{\mathbf{n}} = \mathbf{v} = \nabla n \cdot \hat{\mathbf{n}} = T = 0$ on the conducting surfaces. The vacuum magnetic fields from coils are assumed to have soaked through the bounding surfaces. The computational grid has been constructed to conform with the conducting surfaces bounding the domain of the plasma gun and flux

conserver. The simulations presented use bicubic and biquartic finite elements to represent the poloidal variations (here we typically use 24 elements in the direction normal to the electrodes and 32-48 elements parallel to the electrodes) and various choices for the number of toroidal Fourier modes.

The parallel and perpendicular thermal diffusivities are $\chi_{||} = 387 T^{5/2}$ m^2/s and $\chi_{\perp} = 0.50 T^{-1/2} B^{-2}$ m^2/s (B in Tesla) or a prescribed constant based on electrons and ions, respectively, for a hydrogen plasma at n=5×10^{19} m^{-3}.[10] The numerical computation of $\chi_{\perp}$ is simplified by using the toroidal average of the evolving temperature and magnetic induction fields. However, we usually set $\chi_{\perp}$ to a constant value motivated by experimental measurements and calculations with the CORSICA transport and equilibrium code.[11] Similarly, the electrical diffusivity is computed as $\eta/\mu_0 = 411(1\text{ eV}/T)^{3/2}$ m^2/s, using the toroidally-averaged temperature. (Numerical tests show no significant deviation from results with a 3D computation of resistivity in the conditions of interest.) We have typically employed an isotropic viscosity (ν) of 100-1000 m^2/s, which is used to provide nonlinear numerical stability during the full-power stage of the current drive. However, in this study we will also examine the sensitivities to the value of the scalar viscosity and to using a simple, anisotropic model for the viscosity. With temperatures of approximately 30 eV in the edge plasma or during the spheromak formation stage, and up to a peak of ~200 eV in simulations of decay, the Lundquist number (computed as $S = \mu_0 R v_A/\eta$, where R is the radius of SSPX and v_A is the Alfvén speed) is of order 10^5-10^6. This is much larger than values considered in our earlier spheromak simulations, but the magnetic Prandtl number ($\mathrm{Pm} \equiv \nu\mu_0/\eta$) is also larger for

nonlinear numerical stability purposes.[4,5] The diffusion term in Eq. (1) keeps the density relatively smooth in the absence of particle transport and atomic fueling effects that are poorly understood and not present in the MHD model. The value of the artificial diffusivity (D) is selected to help keep the computed minimum of the number density field above zero during strong drive when the MHD activity is violent. For the same reason, the diffusivity is increased locally in computational cells where n falls to 3% of its volume-averaged value. Use of artificial density diffusivity alters the physics of the simulation and affects energy conservation.[12] We have varied the value of D to determine its influence on the simulation results, however, and find its effects to be small. Because the radiation power is small compared to ohmic power in most SSPX shots after proper wall conditioning, radiation is not modeled in the NIMROD simulations.

In conditions with sustained coaxial electrostatic drive, the cold edge plasma impedes parallel thermal conduction to the wall, despite the chaotic magnetic topology, allowing the plasma core temperature to reach tens of eVs. Magnetic reconnection occurs rapidly in the cold outer plasma. When the drive is temporarily removed, relatively symmetric closed flux surfaces form following the resistive decay of symmetry-breaking modes, and core temperatures increase toward 100 eV or more. Applying a second, long current pulse (sustainment pulse) at currents below a formation threshold,[13] as in many SSPX discharges,[2,14,15] improves performance by delaying the onset of MHD modes that are resonant in the closed-flux region,[6] and higher toroidal-current increases magnetic fields, and larger volumes of closed flux can be achieved.[16] The simulations reveal the sensitivity of the magnetic surfaces and the energy confinement with respect to symmetry-breaking magnetic fluctuations and the close coupling of the magnetics and

energy transport. We have presented detailed comparisons of nonlinear simulations with laboratory measurements from SSPX[2] and assessed confinement properties of the magnetic configuration in Refs. 6-8. In this paper, we present additional comparisons of NIMROD simulation results to SSPX observations, and we assess sensitivities through simulations in which physical and numerical parameters have been varied. The simulation results here and in Ref. 6-8 show that magnetic fields and fluctuation amplitudes agree relatively well with SSPX observations, and temperature evolution data agrees at least qualitatively with experimental behavior.

Figure 1 shows results from a NIMROD simulation that are typical of its use in modeling entire discharges in the SSPX experiment. Here we see a simulation in which a recently installed, 32-module capacitor bank has been used to drive higher currents in the spheromak resulting in higher magnetic fields. NIMROD was modified to incorporate the external LRC circuit equations for the modular capacitor bank. In complete analogy with the SSPX experiment, the inductance, resistance, capacitance and time delay parameters for each module in the capacitor bank are selected as input so that various input current waveforms can be programmed. This bank is connected across the spheromak in parallel with the original "sustainment bank." The latter is a pulse-forming network that is modeled as a known, time-dependent current pulse. The NIMROD simulation can thus legislate the same power-supply impedance as a given experimental discharge. The plasma response in the simulation then produces the current, voltage, and magnetic time histories. The particular NIMROD simulation displayed was undertaken several months before the first exercise of the new capacitor bank. We note that the SSPX data shows that with higher injected gun currents, higher edge magnetic fields are

achieved. The SSPX programmed current in discharge #16538 with the new capacitor bank had a shorter pulse duration and was approximately 70% of the peak current programmed in the NIMROD simulation, and the magnetic field was correspondingly lower. The voltage spikes during formation are similar.

The paper is organized as follows. Section II contains a description of simulations directly modeling spheromak formation. Section III describes simulations of controlled spheromak decay and how physical and numerical parameters affect the simulation results. Comparisons are made to experimental observations in the SSPX spheromak: the simulation results agree well with many features in the SSPX data and qualitatively or semiquantitatively with others. We conclude with a brief summary in Sec. IV.

II. SPHEROMAK FORMATION

The formation of a spheromak in SSPX is initiated by the injection of gas into the coaxial gun in the presence of a bias (poloidal) magnetic field, with an electrical breakdown following the application of high voltage across the coaxial gap. The increasing discharge current generates a toroidal magnetic field with a magnetic pressure somewhat in excess of the tension of the poloidal field, resulting in an ejection of the field into the flux-conserver volume. The resulting plasma pinches about the geometric axis, resulting in an unstable $n = 1$ (toroidal) mode which grows until the broken azimuthal symmetry results in magnetic reconnection which converts some of the injected toroidal magnetic flux into poloidal flux. The result in the presence of flux-conserving walls yields the spheromak magnetic configuration.

Resistive MHD simulation of formation in a pillbox geometry yielded a clear demonstration of the pinching and subsequent spheromak formation,[4] and a simulation of SSPX[8] yielded good agreement with the formation phase of the experiment including cathode voltage spikes associated with the reconnection events and the generation of poloidal magnetic field. However, these simulations did not examine in depth the sensitivity of the results to the viscosity, the maximum toroidal mode number, n_{max}, the plasma density, and other parameters. Several results are presented here with these quantities varied, with the goal of determining the corresponding sensitivities in the spheromak formation. The results also help clarify the physics of the formation phase. Table 1 lists the basic parameters for each of these simulations.

The electrical breakdown process cannot be handled in the model; instead, an initial background plasma is assumed. As will be seen below, the comparison of simulation and experiment is good despite this assumption and the large density diffusion coefficient (10^4 m^2/s in these formation calculations).

A. Experimental observations

Before examining formation simulations, we present results from two discharges in SSPX. Figure 2 shows the time history of a formation pulse, with magnetic probes on the gun and flux-conserver walls showing the propagation of the magnetic field from the coaxial region into the main flux conserver. The perturbed field appears at a probe near the midplane 45 μs after breakdown. The formation in this shot is not fully symmetric, as seen in Fig. 2c; two magnetic probes separated by 202° on the outer wall in the coaxial gun show a clear difference in their magnetic signals before plasma ejection. In contrast,

the shot shown in Fig. 3 shows almost identical fields at the two probes prior to ejection. The difference is reflected in the cathode voltage pulse immediately following ejection.

As will be shown in the simulations discussed later, the rapid change in geometry as the plasma is ejected from the gun is accompanied by a corresponding change in gun inductance which generates a corresponding gun voltage, as seen in Fig. 3. When the current is asymmetric, the current is localized and the inductance is likely already large before ejection from the gun, thereby reducing or eliminating the voltage pulse. It needs to be emphasized, however, that in the experiment breakdown and other processes during this initial formation stage are complex and poorly constrained. As a result, the detailed voltage time history varies more shot-to-shot than this simple description implies. These details are not modeled in the simulations.

The n=1 mode can be seen clearly on the probes in the gun and on *mp090p17* at the bottom of the flux conserver, but is quite weak at the midplane probe, *mp090p09*. This midplane magnetic field is also "measured" in the simulations and plays a critical role in understanding spheromak formation.[8,16]

B. Ejection from a coaxial gun

In the experiment, the breakdown processes often generate initial asymmetries. However, the initial amplitudes of the non-axisymmetric modes in the NIMROD simulations are usually small. As a result, their amplitude is negligible during the ejection of plasma from the gun and a voltage pulse is seen as in the experimental shot shown in Fig. 3. An example is shown in Fig. 4 which shows a clear correlation between the time of ejection of plasma and the voltage pulse in a simulation. (Simulation *lam07*, discussed later, had larger initial amplitudes and no initial voltage pulse, [8] consistent with

the discussion of experimental data.) The time to the voltage peak is thus a measure of the time at which the plasma "bursts" from the gun. From the poloidal flux contours in Fig. 4 it is clear that until after ejection, the gun current flows in a narrow layer between the injected toroidal magnetic field and flux and the compressed poloidal field ahead of this advancing front. This characteristic has also been observed during SSPX formation in using magnetic probes.[17] The time for an Alfvén wave to propagate the length of the gun is one to a few μs, and the plasma pressure is low, so the magnetic forces on the current are in near-balance. The rapid change in geometry as the plasma is ejected from the gun is apparent in Fig. 4b; the voltage pulse in Fig. 4a corresponds in time to the ejection as discussed in the experimental data section.

Results from a series of simulations are shown in Fig. 5. The time to ejection is only weakly dependent on the viscosity, density, gun length, and maximum toroidal mode number kept in the simulation.

The ejection times in the experimental shots are shorter than the simulated time. At least two effects may contribute to this. First, breakdown in the experiment may occur closer to the gun throat than it does in the simulation. The cusp magnetic field seen in the vacuum flux, Fig. 2a, was added to the original bias poloidal field to make the breakdown more reliable by providing a long path for electrons in the gun which operates at low gas pressure. Breakdown likely occurs near this cusp, whereas in the simulation current starts to flow from the upstream end of the coaxial gun. Second, the initial asymmetry in most experimental shots results in larger local magnetic forces where the current flows; these are likely to equilibrate higher in the gun than in the nearly axisymmetric

simulation. The difference in timing is small, however, and appears to have no significant consequences on the later development of the spheromak.

The comparison between experiment and simulation published in the study of reconnection events[8] had no initial pulse in the simulation. That simulation, *lam07*, differed from the "*Form*" series (Table 1) in the initial ("seed") amplitude of the toroidal modes, with the seed amplitude = 10^{-2} T rather than 10^{-4} T. See Fig. 6 for a comparison of the magnetic energies in the two calculations. These results are consistent with the experimental results shown in Figs. 2 and with the conclusion that the initial voltage transient is sensitive to the extent to which axisymmetry is broken during the ejection from the gun. The data, however, is still limited; and further studies are required to confirm this interpretation.

C. Effects of viscosity and maximum toroidal mode number on poloidal field generation

Following the ejection of flux and plasma from the coaxial gun, the current pinches around the geometric axis; and the n = 1 and other column modes grow until symmetry breaking in the axisymmetric flux-conserving boundary becomes large.[8] The reconnection events cause a relaxation of the field into the spheromak geometry. Although the resulting spheromak is robust, the details of these processes can be expected to be sensitive to the parameters of the simulated plasma.

To examine the effect of viscosity, simulations were run with n_{max}=1 and $n=5\times10^{19}$ m^{-3} but kinematic viscosities of 100 m^2/s and 1000 m^2/s. As seen in Fig. 7 the lower viscosity simulation shows more structure on the voltage. The magnetic field at the midplane flux-conserver wall shows that the n = 1 mode grows more rapidly and has

more structure at lower than at higher viscosity, presumably because the fluid velocity in the simulations is sensitive to viscosity. We interpret the voltage spikes as arising from rapid changes in the spheromak inductance; the higher viscosity slows this change and reduces the spike amplitudes. The development of the axisymmetric (n = 0) magnetic field, however, is not sensitive to the viscosity, as seen in Fig. 8.

Viscosity becomes important when the velocity varies over sufficiently small distances as can be seen from the resistive MHD force equation, Eq. (2). For open field-line plasmas with T ~ 25-40 eV, the speed of sound, $(\gamma p/\rho)^{1/2} \sim 1\text{x}10^5$ m/s; we note from the simulations that flow velocities are the same order, as one would anticipate. The plasma is low β, so the magnetic field is nearly force free and the **jxB** term correspondingly small. Thus, we expect the viscosity to become important on scale lengths ~ $\nu/V \sim 10^{-2}$ m at ν = 100 m^2/s. This is the scale at which current layers are seen for this viscosity[8] and allows for inductance changes on the microsecond time scale as observed in the corresponding simulations.

Formation calculations varying n_{max} from 1 to 10 are compared with experiment in Fig. 9; n_{max} =5 and 10 behave qualitatively differently than n_{max} = 1. Following the initial voltage transient resulting from the ejection of flux from the coaxial gun, the voltage associated with the n_{max} = 1 simulation drops significantly relative to that associated with higher toroidal mode-number simulations. At about 140 μs the n_{max} =1 voltage shows a strong variation in time; examination of the poloidal flux (not shown) shows that the x-point for the mean-field (azimuthally-averaged) spheromak jumps to the vicinity of the cusp in the vacuum bias flux. This abrupt jump does not occur in the higher mode-number studies.

D. Electron temperature

For all the formation cases examined, the electron temperature is in the range 25-35 eV. The magnetic field lines are open to the cathode and flux conserver, so the temperature is determined by thermal parallel conductivity. The lack of sensitivity of the temperature to heating values and detailed geometry results because the thermal conductivity is proportional to $T_e^{5/2}$ and ohmic heating is proportional to $T_e^{-3/2}$, so that small changes in T_e are sufficient to balance any effects of viscosity, mode numbers, etc.

E. Summary: Sensitivities during spheromak formation

Mode number. The initial phase of plasma formation in the coaxial gun and its injection into the flux conserver are insensitive to the maximum mode number assumed in the simulations. The amplitudes of modes with $n \geq 1$ remain low during this time.

The gun voltage during ejection of plasma from the coaxial region is found to vary with the symmetry of the breakdown and other parameters. Although the resulting detailed time history is affected, the final spheromak is not significantly changed by the initial symmetry.

If the maximum toroidal mode number is set to 1, the bias poloidal flux is amplified and a mean-field spheromak is formed. However, once reconnection becomes significant the time history of the formation magnetic field and gun voltage differ considerably from experiment and from those when n_{max} = 5 or 10 are assumed in the simulation. The histories are almost identical for these two simulation cases.

Viscosity. The primary effect of viscosity in the range of 10 m^2/s to 1000 m^2/s is on the detailed time histories, for example, the magnetic field and gun voltage histories. The amplitude of the voltage spikes is sensitive to the viscosity. Although these details are

important for comparing with and interpreting experimental results, they are found to have little impact on the mean-field spheromak parameters, e.g. the magnetic field strengths.

Density. The density in the simulation has only minor effects on spheromak formation. Although it affects Alfvén times, these are an order of magnitude less than the evolution time of the mean field; and plasma resistivity is not playing a role in the dynamics, so changes in the Alfvén time are not important at the global level. Plasma inertial effects are small.

Electron temperature. Because of the strong dependence of the parallel (to magnetic field) electron thermal conductivity on T_e, the T_e produced during formation is insensitive to the experimental and simulation discharge parameters. As a consequence, the Lunquist number is insensitive to the precise values of the parameters in the simulation.

III. CONTROLLED DECAY

We have undertaken a suite of simulations in which we have examined in a limited way the influence of a few of the physical and numerical parameters on the evolution of the magnetics and the electron temperature. We have varied the effective ionization state, Z_{eff}, which influences the resistivity and the parallel thermal conduction, the background electron number density, the scalar kinematic viscosity, the artificial density diffusivity, the toroidal mode resolution, and the poloidal resolution. We examine the influence of these parameter variations on the comparisons of the simulation magnetic and electron temperature evolution with the data observed in the SSPX experiment. We

have also examined the sensitivity of the NIMROD simulation results with respect to using a tensor model of the plasma viscosity.

A. Effects of ionization state, scalar viscosity, plasma density, and density diffusivity

In the NIMROD fluid model there are a number of important parameters to be set that affect coefficients in the system of equations. The choices of these parameters is guided by experimental data and by inferences drawn from modeling the experimental data. Here we consider limited variations in $Z_{\rm eff}$, the background electron number density, the scalar kinematic viscosity, and the artificial density diffusivity. Before showing the results of the parameter studies, we first discuss some of the physics associated with these parameters.

The effective ionization state of the plasma directly affects the electron-ion collision rate and, hence, the plasma resistivity and electron parallel thermal conductivity.[9,18] Increasing $Z_{\rm eff}$ increases the electron-ion collision rate, increases the electrical resistivity, and decreases the electron parallel thermal conduction, *e.g.*, increasing $Z_{\rm eff}$=1 to $Z_{\rm eff}$=2.3 increases the resistivity by ×2.3 and decreases the parallel thermal conductivity by ×0.71 Considering Eq. (3) for the electron temperature evolution, for fixed current density and magnetic field structure, an increase in the resistivity η and decrease in thermal conductivity $\chi_{\|}$ might be expected to increase the electron temperature. However, the evolution of the magnetics, the fluid motion, and the electron temperature are strongly coupled. Moreover, the electron temperature evolution in our spheromak simulations is very sensitive to the quality of the magnetic surfaces,[5-8] which in turn is very sensitive to the amplitudes of symmetry-breaking magnetic perturbations at levels $|\delta B/B_0|$ less than or equal to a few percent.[7,8,19]

If the spheromak is limited by a power flow limit or a plasma stability limit that depends on $\beta=8\pi n_e T_e / B_0^2$, then if the average electron number density n_e is reduced, T_e might be expected to increase if the magnetic structure is unchanged. However, if the plasma number density is reduced, then the inertia term in the momentum equation, Eq.(2), is reduced, which in turn increases ideal magnetohydrodynamic growth rates. This can be deleterious to maintaining good magnetic surfaces because magnetic islands and stochastic field lines degrade the electron temperature owing to the enormous anisotropy, $\chi_{\|}/\chi_{\perp}>>1$.

We have used values of the scalar kinematic viscosity ν=500 or 1000 m^2/s in many of our NIMROD simulations. The non-dissipative algorithm in NIMROD requires physical viscosity to limit the development of small-scale structures that cannot be resolved; simulations fail to converge in the absence of a sufficient viscosity. Evaluation of the Braginskii[9] tensor model for the viscosity yields parallel viscosity values $\eta_0/\rho \sim 10^6 m^2/s$ and perpendicular viscosity values $\eta_1/\rho \sim 10^{-1} m^2/s$ for T_i = 150 eV, n = 3.5×10^{13} cm^{-3}, and B = 0.5 T. The scalar viscosity used in the simulations therefore falls somewhere between the extremes. However, viscosity has a stabilizing influence for MHD modes, and the scalar-viscosity modeling may reduce symmetry-breaking magnetic perturbations that govern energy transport and the resulting temperature profile.

The artificial density diffusivity D in Eq.(1) affects the MHD physics in several ways as described in Ref. 12. The role of D is to maintain a relatively smooth plasma density, particularly during the violent formation stage of the spheromak. In the absence of good models for plasma sources (from bounding surfaces or ionization of neutral gas in the volume), we initialize a plasma density throughout the domain and use the density

diffusivity to moderate the evolution of the plasma density. A direct consequence of the artificial diffusivity is that the evolution of the internal energy density acquires a fictitious term $3TD\nabla^2 n$ that is a sink where the density peaks at the magnetic axis of the spheromak:

$$\frac{\partial 3nT}{\partial t} + \nabla \cdot (3nT\mathbf{V}) + 2nT\nabla \cdot \mathbf{V} = \frac{1}{2}\eta J^2 + \nabla \cdot n\vec{\vec{\chi}}\nabla T + 3TD\nabla^2 n \qquad (6)$$

This aspect of the modeling may artificially reduce the peak plasma temperature near the magnetic axis.

A suite of NIMROD simulations (*lam07* variants on the *lam06* simulation in Ref. 7) investigates sensitivity to the values of scalar viscosity, artificial particle diffusivity, Z_{eff}, and number density. Figures 10 and 11 show the evolution of the poloidal magnetic field at the outboard midplane of the flux conserver and the peak electron temperature from the simulations, each of which requires several weeks of run time on a local Beowulf cluster. The highest poloidal magnetic field occurred in the simulation with the lowest Z_{eff}=1 and therefore smallest resistivity (*lam07* in Fig. 10). (Viscosity has little effect on the buildup of the azimuthally averaged field, as seen in Fig. 8.) The other magnetic field traces in Fig. 10 do not show strong dependences on the parameter variations and are in general agreement with typical SSPX data for discharges with similar gun current. In contrast, the peak temperature histories for this series of simulations show considerably greater variation in Fig. 11, and there is also considerable spread in the SSPX temperature data. As has been established in earlier experimental and simulation work, [4-8,11,14,15,18] the plasma energy confinement and temperature are quite sensitive to the quality of the magnetic surfaces, which are profoundly influenced by the amplitudes of the symmetry-breaking magnetic perturbations at small amplitudes (a few percent or less). The time

histories of the finite-*n* magnetic fluctuations in the simulations corresponding to those in Fig. 11 differ significantly during controlled decay accounting for the observed differences in the temperature histories. The stochasticity of some of the magnetic field lines is an important factor influencing the transport, the electron temperature, the resistivity, and the magnetohydrodynamics in the strongly coupled system.

The plasma temperatures in the simulations get as high as 150eV in this series, while the SSPX temperatures in similar discharges exceed 200eV. The experiments exhibiting the highest electron temperatures tend to confine energy somewhat better than is suggested by NIMROD in this series of simulations. However, there are many SSPX discharges with electron temperatures in the range 100ev to 150eV for similar injected gun current histories. Given the extreme sensitivities of simulating the plasma temperature evolution in NIMROD and the limitations due to both finite computing resources (which restricts our attempts to examine numerical convergence as rigorously as we would like) and the simplifications of our resistive MHD physics model, our expectations on how close the simulations should agree with experiment on the temperature evolution should be tempered. Certainly the agreement shown here and in our earlier work[6-8] on the magnetics and voltages tends to be good; the agreement on temperature is better than just qualitative; and the gross behavior with respect to the importance of the *n*=1 mode in formation, the relationship of the current-profile evolution to the emergence of symmetry-breaking modes which then influences the magnetic confinement, [2,11,14-16] and the ultimate crash of the discharge when the current profile sags at the edge leading to *n*=2 mode activity seen in the experiment[2,11,14-16] are confirmed by the simulations.[5-8]

Figure 12 shows the results of restarting simulation *lam07znn* at t~0.5ms after formation and reducing D from 10000 to 100 m^2/s in *lam07znd*: T_e rises faster to ~160 eV at t~2ms and grows to >180eV after 3.5ms, before small-amplitude magnetic fluctuations (n=2) degrade the magnetic surfaces and the discharge crashes. In these simulations the density is allowed to evolve after the formation phase, and we observe a rather weak peaking of the density near the magnetic axis. The reduction of the value of D reduces the energy sink near the magnetic axis, which in turn does allow a somewhat higher plasma temperature to be achieved. However, the magnetic fluctuation histories do not remain unaffected and strongly influence the energy confinement. In Fig. 11 only higher values of D~10^4 m^2/s are shown, and the NIMROD simulations predicted lower temperatures than those observed in the SSPX data.

B. Effects of poloidal resolution

Numerical accuracy in SSPX simulations depends on the ability to resolve the MHD modes, their effect on magnetic topology, and the anisotropic thermal conduction along evolving and sometimes chaotic field-lines. Sensitivity to error is heightened by the feedback of transport-inducing fluctuations on the evolving profiles that influence the MHD activity. To check the level of numerical error during the controlled decay phase of simulations for the new SSPX capacitor bank, we have undertaken a series of calculations, changing finite element basis functions and isolating transport physics. We generally retained toroidal modes $0 \le n \le 5$ and a poloidal resolution of 24×48 elements in a mesh whose boundaries conform smoothly to the conducting surfaces bounding the spheromak. In some of the simulations, however, we restricted the toroidal resolution to just n=0 after formation to ensure perfect magnetic surfaces so as to obtain an upper limit

on the energy confinement. We also investigated changing the value of the perpendicular thermal diffusivity ($\chi_\perp$) from 20 m^2/s to 1 m^2/s to 0 m^2/s to understand the influence of these changes on the simulated temperature evolution.

When changing the finite element bases from bicubic to biquartic polynomials in the full simulations, we find quantitatively small changes in magnetic profiles but significant discrepancies with respect to energy confinement. The *newbank1a* simulation completed with bicubic elements is refined to use biquartic elements in simulation *newbank1b* for the sensitive quiescent phase starting at 2 ms. After approximately 1500 Alfvén times, traces of the edge magnetic field are not distinguishable, and the safety factor and parallel current profiles agree to within 10% over most of the profile (Fig. 13). Nonetheless, the biquartic computation does not maintain a state of high confinement as long as predicted in the bicubic computation, as shown in Fig. 14. At 3 ms, the value of the peak temperature obtained in *newbank1b* drops slightly to 230 eV, and after 4 ms, it drops to approximately 100 eV. In contrast, the peak in *newbank1a* continues climbing to 370 eV before it drops at 5 ms.

An important consideration when modeling extremely anisotropic transport—and the ratio of thermal conductivities ($\chi_{||}/\chi_\perp$) exceeds 10^6 in SSPX plasmas with $T_e > 100$ eV—is whether perpendicular transport is numerically enhanced by truncation error. The performance of high-order finite elements in resolving extremely anisotropic thermal conduction has been investigated in Ref. 9 in a two-dimensional calculation with a fixed magnetic structure. Favorable numerical behavior is reported for bicubic and biquartic finite elements for grid resolutions and $\chi_{||}/\chi_\perp$ values comparable to those in our SSPX

simulation. However, here we include the additional complexity of the self-consistent evolution of the magnetics.

To investigate the accuracy of energy transport in simulations for the new capacitor bank, we varied $\chi_{\parallel}/\chi_{\perp}$ and the artificial density diffusivity in bicubic computations, evolved temperature alone in bicubic and biquartic computations, and compared fluctuation-free results with a 1D model. In a bicubic simulation with $\chi_{\perp}$=20 m^2/s that is not shown in Fig. 14, temperatures reached 190eV in contrast to the 370eV result with $\chi_{\perp}$=1 m^2/s. Had the numerically computed temperature and energy confinement been insensitive to perpendicular thermal conductivity during this quiescent phase, it would have been a clear indication that errors from modeling the large parallel diffusivity are polluting perpendicular transport. (Modeling of the energy confinement in SSPX with the CORSICA code supports values of $\chi_{\perp}$=1 m^2/s during controlled decay in SSPX when the highest plasma temperatures are observed.[10]) Regarding artificial particle diffusivity, a bicubic computation with $\chi_{\perp}$=1 m^2/s and D reduced by two orders of magnitude (*newbank1ad* in Figs. 13 and 14) nearly matches the *newbank1a* result until an earlier thermal collapse occurs at 4.5 ms. Another pair of computations compares bicubic and biquartic resolution when evolving temperature and its effect on thermal conductivities and Ohmic heating in the presence of fixed profiles of n, **B**, and **V**. They are started from 3 ms into the *newbank1a* bicubic computation, and the resulting internal energies only differ by a small and relatively constant offset, as shown in Fig. 15. Moreover, peak temperatures of 246.0 and 247.4 at the end of the thermal computations agree to within 1%.

Returning to analysis of the full simulations, we note that while the symmetry-breaking magnetic fluctuation amplitudes are small and the magnetic confinement is good, the temperatures in the bicubic *newbank1a* track values computed from a one-dimensional model. The 1D calculation solves

$$\tfrac{3}{2} n k_B \frac{\partial}{\partial t} T = \nabla \cdot n k_B \chi_\perp \nabla T + \eta(T) J(t)^2 / 2 \qquad (7)$$

assuming perfect magnetic surfaces and using a time dependence for the plasma current that mimics the time dependence of the current decay in the NIMROD simulation for t > 2ms. The coefficients have $\chi_\perp$=0 or 1 m^2/s, and η is the classical Spitzer-Braginskii temperature-dependent resistivity. When only the n=0 component of the magnetic field is retained for t > 2ms in a bicubic NIMROD simulation (*newbank1a0*), the resulting temperature trace tracks the one-dimensional model for an even longer time (Fig. 14) and establishes a prediction for an upper limit on the plasma temperature that might be achieved in SSPX up to a given time in the discharge if the magnetic surfaces remain good. These results also provide confidence in the poloidal resolution of anisotropic thermal conduction with the mesh of bicubic elements.

Having shown that the bicubic elements represent anisotropic transport with reasonable accuracy, we infer that differences in the MHD activity must indirectly account for the energy confinement discrepancy between *newbank1a* and *newbank1b*. Evidence is found in the magnetic fluctuation energy histories, shown in Fig. 16. We first note that the n>1 fluctuation energies are at least an order of magnitude smaller than the internal energy, and the discrepancy between the two simulations is mostly a matter of detail until just before 3 ms for n>2 and throughout the plotted time for n=2. Neither the n=2 fluctuation nor the n=1 fluctuation (not shown) are resonant within the core

plasma ($\Psi > 0.2$ in Fig. 13) during this period of time. The n=1 fluctuation energy is an order of magnitude larger, but like the n=2 evolution, there is reasonably good agreement between the bicubic and biquartic results. Unlike the n=1 column mode and its n=2 harmonic, the n=5 mode shows distinct behavior in the biquartic computation starting at 2.9 ms, followed by n=4 excitation at 3.1 ms. The q-profile evolution has $q > 4/5$ at 2.2 ms, dips below 4/5 at $\Psi \cong 0.25$ by 3 ms, and decreases below 3/4 by 3.5 ms, which is shown in Fig. 13. The biquartic computation thus finds instability when the respective modes become resonant, unlike the bicubic computation, and as evident in Fig. 17, this leads to a larger region of magnetic stochasticity inside the location of minimum q-value. This is also the period of time when the peak temperature of *newbank1b* falls below that of *newbank1a* in Fig. 14. Figure 16 shows that the n=3 mode starts growing at 3.5 ms in the biquartic computation. Its saturation leads to the thermal collapse at 4 ms. The q-profile evolution in *newbank1a* trails that in *newbank1b* slightly, and the parallel current profile has less of a gradient in the outer region of the core plasma, possibly due the absence of n=4-5 activity. The delayed excitation of the n=3 in the bicubic computation may be related to these profile differences, but less poloidal resolution may also contribute. On a more qualitative level, excitation of the n=3 eventually leads to the thermal collapse in both computations.

While the discrepancies between the bicubic and biquartic computations indicate a need for greater numerical resolution, the biquartic simulation is already very intensive for our Beowulf cluster. More importantly, there is still something to be learned from the results we have obtained. First, sensitivity of energy confinement to excitation of resonant MHD modes is in general agreement with experimental results[11] and likely

contributes to the spread in laboratory data shown in Fig. 11, for example. Second, the NIMROD simulation without magnetic fluctuations suggest that T_e > 450eV can be achieved with good control over the magnetic fluctuations, and SSPX has obtained electron temperatures approaching 500eV with the new capacitor bank.[3] Finally, while the overall evolution of energy confinement agrees at least qualitatively with the experiment, the trend with increasing resolution is toward lower peak temperatures than what is achieved in experiment. This points to an inadequacy of the MHD model with collisional transport for the conditions achieved in recent SSPX discharges.

C. Effects of tensor viscosity and variations in kinematic viscosity

Kinematic viscosity, ν, is used in NIMROD, Eq.(2), both to smooth fine-grained structures and to provide a boundary layer of finite volume on the surfaces of the spheromak electrodes.[4] In this boundary layer the magnitude of kinematic viscosity is increased in SSPX calculations by a factor ≈30 above its value in the volume.

Actual viscosity in the plasma is extremely anisotropic and differs significantly from the functional form of the kinematic viscosity described above. The version of the code used in these calculations allows parallel viscous stress that is in the Braginskii form albeit with a coefficient that is independent of the plasma parameters. The form of the viscous force available for the simulations is thus

$$\mathbf{F}_{visc} = \nabla \cdot \nu\rho\nabla\mathbf{V} - \nabla \cdot \mathbf{P}_{||} \tag{8}$$

where

$$\mathbf{P}_{||} = -\eta_0\left(\hat{\mathbf{b}} \cdot \nabla\mathbf{V} \cdot \hat{\mathbf{b}} - \frac{1}{3}\nabla \cdot \mathbf{V}\right)\left(3\hat{\mathbf{b}}\hat{\mathbf{b}} - \mathbf{I}\right) . \tag{9}$$

The Braginskii coefficient is a function of the plasma parameters:

$$\eta_0 = 0.96 n k_B T_i \tau_i \tag{10}$$

with the temperature in eV and

$$\tau_i = 2.09x10^{13} T_i^{3/2} \mu^{1/2} / n \ln \Lambda \qquad (11)$$

The density, n, is in MKS, and $\mu = m_i / m_p$. Evaluating η_0 at the representative parameters: T_i=150 eV, n=3.5x10^{19} m^{-3}, and μ=1, yields $\eta_0 / n m_i$=1.1x10^6 m^2/s.

To evaluate effects of anisotropic viscous stress, a series of simulations were made with and without the parallel viscosity and kinematic (essentially perpendicular) coefficients of ν=10 m^2/s, 100 m^2/s, and 1000 m^2/s. Other varied parameters were the number of toroidal modes and the particle diffusion coefficient. The effect of adding the large parallel viscosity is shown in Fig. 18, which compares the q-profiles at ν=1000 m^2/s with and without the parallel viscosity. The added viscosity shifts and broadens the minimum of q after about 2 ms. Reducing the kinematic viscosity to 10 m^2/s has a much larger effect, as also seen in the figure. The quality of the magnetic surfaces is sensitive to these changes, and a reflection of this effect is seen in Fig. 19; however, results of the previous section lead to resolution concerns for simulations with reduced values of perpendicular viscosity.

In these runs the relatively small particle diffusion coefficient of 100 m^2/s reduced the density in the bottom of the coaxial gun by about a factor of 20 relative to calculations with a much larger diffusion coefficient (e.g. 10000 m^2/s).

The effect of parallel viscosity on the density was examined by setting n_{max}=0. The primary effect was to spread a density peak that exists near the top of the gun close to the magnetic axis, with no significant consequences.

A rotation boundary condition is applied to all these simulation to give a mode frequency of about 10^4 Hz; evidently the dominant plasma rotation mechanism in the

laboratory plasma is not MHD in nature. The resulting rotation is nearly rigid rotation at 1000 m^2/s, where as at 10 m^2/s the effect of the magnetized plasma is to yield a drop of about half the rotation near the flux-conserver wall.

Finally, a scaling of mode magnetic energies (n_{max}=20) was made for kinematic viscosities from 10 m^2/s to 1000 m^2/s (Table 2). As seen in Fig. 20, in each case there is a rapid drop in mode energy above n=5 to 7. Only small changes in the q-profile are seen for the three cases.

This reduction of energy with mode numbers indicates that simulations with n_{max} =5 capture the dominant spheromak physics, especially for ν=100-1000 m^2/s. This result is consistent with experiment, in which mode numbers above 4-5 usually have small amplitudes. Parallel viscosity has quantitative effects, especially on the quality of mode surfaces and the electron temperature, but otherwise has little effect on the mean-field spheromak.

IV. SUMMARY

In this paper, we have presented selected parameter studies of spheromak plasma formation and controlled decay using NIMROD simulations and have compared selected results to SSPX observations. The simulations illuminate the sensitivities of the physics with respect to variations in physical and numerical parameters. The simulation results presented here and in previous publications show that magnetic fields and fluctuation amplitudes agree relatively well with SSPX observations, and temperature evolution data agrees at least qualitatively with experimental behavior. The comparisons of the simulation temperature evolution are at best semi-quantitative, and we are unable to

demonstrate numerical convergence of the detailed evolution of high-*n* symmetry-breaking fluctuations and their effect on plasma temperature during the quiescent phase of the spheromak evolution. The presence of some stochastic field lines and the close coupling of the system of governing equations contribute to the difficulty of achieving strict numerical convergence of all of the detailed time histories in the simulations. Similar effects may play a role in the observed shot-to-shot variations seen in the SSPX experiment. However, the information described in Section IIIB indicates that the MHD/collisional transport model predicts more fluctuation activity and less energy confinement than what is achieved in the experiment. The importance of flux-limiting effects beyond the scope of collisional transport are presently being investigated through integral closures.[20,21] The possibility of drift effects in the experiment leading to greater stability of the symmetry-breaking modes is a topic for future modeling efforts, and numerical development for Hall, gyroviscous, and magnetization heat-flow effects is underway. Relaxing the assumption of rapid electron-ion thermal equilibration is also worth investigation.

Nevertheless, the simulations described here capture the most important features of the gross behavior of spheromak formation and controlled decay. In particular, the buildup of the azimuthally averaged field is fairly robust with respect to variations in plasma density, viscosity, and maximum toroidal mode number despite significant variations in detailed time histories of, e.g., reconnection events. These results suggest that spheromak field buildup is insensitive to the details of the physics in the reconnection layers, although more detailed physics studies with two-fluid and other models will be required to substantiate this.

Another important feature in which NIMROD simulations and the SSPX experimental data are consistent is that when driving the spheromak with electrostatic helicity injection, by relaxing and tailoring the drive during partial decay, good magnetic surfaces form and energy confinement improves until such time as symmetry breaking magnetic fluctuations degrade the surfaces and the confinement. The simulations and experimental results elucidate the interrelation of the current-profile evolution, the emergence of magnetic fluctuations that are associated with specific resonance surfaces that appear in the plasma, and the effects of the fluctuations on the quality of the magnetic surfaces and the energy confinement in what is a closely coupled system.

ACKNOWLEDGMENTS

We are grateful to L.D. Pearlstein, T.K. Fowler, L.L. LoDestro, E.D. Held, J.-Y. Ji, members of the SSPX experimental team at Livermore, and the NIMROD team for support, helpful discussions, and encouragement. The simulations made use of resources at the National Energy Research Supercomputer Center under Department of Energy Contract No. DE-AC03-76SF00098. This work was performed under the auspices of the U.S. Department of Energy partly under contracts W7405-ENG-48 and DE-AC52-07NA27344 at the Lawrence Livermore National Laboratory and grant FG02-01ER54661 at the University of Wisconsin-Madison.

Table 1. Parameter variations in Nimrod runs. All these simulations used bicubic finite elements, Z_{eff} = 1, there was no parallel viscosity, the perpendicular thermal conductivity was 20 m^2/s and the particle diffusivity was 10^4 m^2/s.

Run name	L_{gun}	**Density**	n_{max}	**Viscosity**	**Comments**
lam07	0.6	5e19	5	100 , t<354 μs, 500, t>354 μs	I_{gun} fit to experiment; 465 kA at 115 μs. Initial mode amplitudes 100 times greater than in the Form-series of simulations
Form	0.60	$1.5x10^{20}$	10	1000	V_{cap}=6.8, Formation pulse
Form0.1	0.25	$1.5 x10^{20}$	0	1000	V_{cap}=6.8, Formation pulse
Form0.2	0.35	$1.5 x10^{20}$	1	1000	V_{cap}=6.8, Formation pulse
Form0.3	0.35	$1.5x10^{20}$	1	1000	V_{cap}=6.8, Formation pulse
Form0.4	0.40	$5 x10^{19}$	1	1000	V_{cap}=6.8, Formation pulse
Form0.5	0.40	$5 x10^{19}$	1	1000	V_{cap}=8.0, Formation pulse
Form0.6	0.40	$5 x10^{19}$	1	100	V_{cap}=8.0, Formation pulse
Form0.7	0.40	$5 x10^{19}$	10	100	V_{cap}=8.0, Formation pulse
Form0.8	0.40	$5 x10^{19}$	5	100	V_{cap}=8.0, Formation pulse
Form0.9	0.40	$5 x10^{19}$	5	1000	V_{cap}=8.0, Formation pulse

Notes: The gun solenoid currents in the Form-series of simulations were identical, generating a total bias flux within the coaxial gun of 35 mWb for the gun length, L_{gun}=0.4m.

Table 2. Parameter variations in Nimrod runs. For these simulations, L_{gun}=0.6 m, n=3.5x10^{19} m^2/s, parallel viscosity = 1.1x10^6 m^2/s, the perpendicular thermal conductivity = 1 m^2/s, and bicubic finite elements were used.

Run name	n_{max}	**Viscosity**	**D**	**Comments**
K_v=1000_n=0	0	1000	100	
K_v=10_n=0	0	10	100	
Kin_visc=0.1	5	0.1	100	Failed to converge
Kin_visc=10	5	10	100	
Kin_visc=1000	5	1000	100	
Kv=e1_n=21	21	10	10000	
Kv=e2_n=21	21	100	10000	
Kv=e3_n=11	10	1000	10000	
Kv=e3+n=21	21	1000	10000	

References

[1] T. R. Jarboe, Plasma Phys. Control. Fusion 36, 945 (1994); T. R. Jarboe, I Henins, A. R. Sherwood, C. W. Barnes, and H. W. Hoida, Phys. Rev. Lett. **51**, 39 (1983).

[2] H. S. McLean, S. Woodruff, E. B. Hooper, R. H. Bulmer, D. N. Hill, C. Holcomb, J. Moller, B. W. Stallard, R. D. Wood, Z. Wang, Phys. Rev. Lett. 88, 125004 (2002); H.S. McLean, S. Woodruff, D.N. Hill, R. H. Bulmer, B. I. Cohen, E. B. Hooper, J. Moller, D. D. Ryutov, B. W. Stallard, R. D. Wood, C. T. Holcomb, T. R. Jarboe, C. Romero-Talámas, P. M. Bellan, 30th EPS Conference on Contr. Fusion and Plasma Phys., St. Petersburg, Russia, 7-11 July 2003, Europhysics conference Abstracts, **27A**, P3.230.

[3] R. Wood, D. N. Hill, H. S. McLean, E. B. Hooper, B. F. Hudson, and J. M. Moller, in preparation.

[4] C. R. Sovinec, J. M. Finn, and D. del-Castillo-Negrete, Phys. Plasmas 8, 475 (2001).

[5] R.H. Cohen, H.L. Berk, B.I. Cohen, T.K. Fowler, A.H. Glasser, E.B. Hooper, L.L. LoDestro, E.C. Morse, L.D. Pearlstein, T.D. Rognlien, D.D. Ryutov, C.R. Sovinec, and S. Woodruff, Nucl. Fusion **43**, 1220 (2003).

[6] C.R. Sovinec, B.I. Cohen, G.A. Cone, E.B. Hooper, and H.S. McLean, Physical Review Letters **94**, 35003 (2005).

[7] B. I. Cohen, E. B. Hooper, R. H. Cohen, D. N. Hill, H. S. McLean, R. D. Wood, S. Woodruff, C. R. Sovinec, and G. A. Cone, Phys. Plasmas 12, 056106 (2005).

[8] E. B. Hooper, T. A. Kopriva, B. I. Cohen, D. N. Hill, H. S. McLean, R. D. Wood, S. Woodruff, and C. R. Sovinec, Phys. Plasmas **12**, 092503 (2005).

[9] C. R. Sovinec, A. H. Glasser, T. A. Gianakon, D. C. Barnes, R. A. Nebel, S. E. Kruger, D. D. Schnack, S. J. Plimpton, A. Tarditi, and M. S. Chu, J Comp Phys. **195**, 355-386 (2004).

[10] S. I. Braginskii, *Reviews of Plasma Physics*, edited by M. A. Leontovich, Vol. 1, p. 205 (Consultants Bureau, New York, 1965).

[11] H. S. McLean, R. D. Wood, B. I. Cohen, E. B. Hooper, D. N. Hill, J. M. Moller, C. Romero-Talamas, and S. Woodruff, Phys. Plasmas **13**, 056105 (2006).

[12] D. D. Ryutov, B. I Cohen, R. H. Cohen, E. B. Hooper, and C. R. Sovinec
Phys. Plasmas 12, 084504 (2005).

[13] E.B. Hooper, D.N. Hill, H.S. McLean, C.A. Romero-Talamás and R.D. Wood Nucl. Fusion **47**, 1064 (2007).

[14] S. Woodruff, D. N. Hill, E. B. Hooper, J. Moller, H. S. McLean, B. W. Stallard, R. D. Wood, R. Bulmer, B. Cohen, Phys. Rev. Lett. **90**, 95001(2003).

[15] S. Woodruff, B. W. Stallard, H. S. McLean, E. B. Hooper, R. Bulmer, B. I. Cohen, D. N. Hill, C.T. Holcomb, J. Moller, R. D. Wood, Phys. Rev. Lett 93, 205002 (2004); S. Woodruff, B.I. Cohen, E.B. Hooper, H.S. McLean, B.W. Stallard, D.N. Hill, C.T. Holcomb, C.Romero-Talamas, R.D. Wood, G. Cone, C.R. Sovinec, Phys. Plasmas 12, 052502 (2005).

[16] A. al-Karkhy, P. K. Browning, G. Cuningham, S. J. Gee, and M. G,. Rusbridge, Phys. Rev. Lett. **70**, 1814 (1993).

[17]C.A. Romero-Talamas, E. B. Hooper, D.N. Hill, B. I. Cohen, H. S. McLean, R. D. Wood, and J. M. Moller, J. Fusion Energy **26**, 169 (2007).

[18] L. Spitzer, *Physics of fully ionized gases* , New York: Interscience Publication, 1965, 2nd rev. ed.

[19] M. V. Umansky, R. H. Bulmer, D. N. Hill, L. L. LoDestro, W. M. Nevins, D. D. Ryutov, S. Woodruff, Plasma Physics and Controlled Fusion **48**, 235-244, (2006).

[20] J.-Y. Ji and E. D. Held, Bull. Am. Phys. Soc. **50**, No. 11, UP8.00014 (2007).

[21] E. D. Held, J. D. Callen, C. C. Hegna, C. R. Sovinec, T. A. Gianakon, and S. E. Kruger, Phys. Plasmas **11**, 2419 (2004).

Figure Captions

Figure 1. (Color online) NIMROD simulation of the modular capacitor bank and representative SSPX data for discharges using the original and new capacitor banks: gun voltage, gun current and poloidal magnetic field at the edge of the midplane in the flux conserver vs. time.

Figure 2. (Color online) (a) SSPX geometry. The vacuum (bias) poloidal magnetic field is shown. Magnetic probes (measuring the field in T) installed in the flux-conserver wall are indicated by plus signs; the probes used in Figs. 2-3 are labeled. (b) Discharge in SSPX showing the movement of plasma down the gun (note probes 2-6). (c) Azimuthally located probes showing asymmetry during plasma ejection from the gun. Probe *mp292p03* (dashed line) is 202° azimuthally from *mp090p03* (solid line), etc.

Figure 3. A formation shot with a high degree of symmetry. Probes as in Fig. 2c. Compare the voltage immediately following the vertical dashed line with Fig. 4.

Figure 4. (Color online) (a) Simulation showing voltage pulse as plasma is ejected from the gun. (b) Development of the poloidal flux ($n = 0$) during the initial stage of formation, showing the abrupt change in geometry as the plasma exits the gun.

Figure 5. (Color online) Time to voltage pulse for various NIMROD parameters. The labels M-U correspond to *Form0.1-Form0.9*; c.f. Table 1.

Figure 6. (Color online) Comparison of the energy in the $n = 0$ and 1 modes for two runs with n_{max}=5 but different initial gun parameters. (See Table 1.) The initial voltage transient was absent in *lam07*.

Figure 7. (Color online) Effect of viscosity. Left, $\nu = 10^3$ m^2/s; right, $\nu = 10^2$ m^2/s.

Figure 8. (Color online) The mean-magnetic field is almost independent of viscosity. Shown are the currents and fields from the cases in Fig. 7.

Figure 9. (Color online) Effect of maximum mode number on detailed time history of voltage and magnetic field. Top, gun voltage; bottom magnetic field.

Figure 10. (Color online) The poloidal magnetic field at the outboard midplane of the flux conserver vs. time in the *lam07* NIMROD series of spheromak simulations. A composite SSPX B_z vs. time trace (dashed line) is plotted for similar gun current input and typical operation with the older capacitor bank.

Figure 11. (Color online) Peak electron temperature vs. time in *lam07* NIMROD series of spheromak simulations

Figure 12 (Color online) (a) Peak electron temperature vs. time. (b) Magnetic energy for toroidal modes integrated over volume vs. time. (c) Electron temperature contours at t=3.66 ms showing the effects of decreasing the density diffusivity.

Figure 13. (Color online) Toroidally averaged edge poloidal magnetic field vs time for several NIMROD simulations. The q and λ profiles as functions of magnetic flux Ψ at t=3.5ms in *newbank1a* and *newbank1b*; note that the magnetic axis is at Ψ=1.

Figure 14. (Color online) Peak plasma temperature vs. time for several NIMROD simulations and for a one-dimensional simplified model assuming perfect surfaces. The brief *newbank1gl* computation is very similar to *newbank1b* and confirms that the biquartic results do not change when the node locations of the polynomial basis functions are moved.

Figure 15. (Color online) Comparison of internal energy evolution from bicubic and biquartic computations that solve Eq. (3) with n, **B**, and **V** fixed at the state achieved at 3 ms in the *newbank1a* simulation.

Figure 16. (Color online) Comparison of the evolution of magnetic fluctuation energy by toroidal Fourier index (n) from the bicubic *newbank1a* (black) and the biquartic *newbank1b* (red).

Figure 17. (Color online) Poincaré surface-of-section plot of the magnetic field lines from NIMROD simulations *newbank1*, *newbank1a* (third-order polynomial) and *newbank1b* (fourth-order polynomial) at various times.

Figure 18. (Color online) The q-profile is affected by parallel viscosity and by reducing the kinematic viscosity. a) $\nu = 1000$ m^2/s. b) $\nu = 100$ m^2/s. c) $\nu = 10$ m^2/s. The volume of "good" surfaces decreases for changes from $\nu = 1000$ m^2/s.

Figure 19. (Color online) Electron temperature evolution for the three cases shown in Fig. 18.

Figure 20. (Color online) Mode amplitude scaling with toroidal mode number for the simulations shown in Fig. 18.

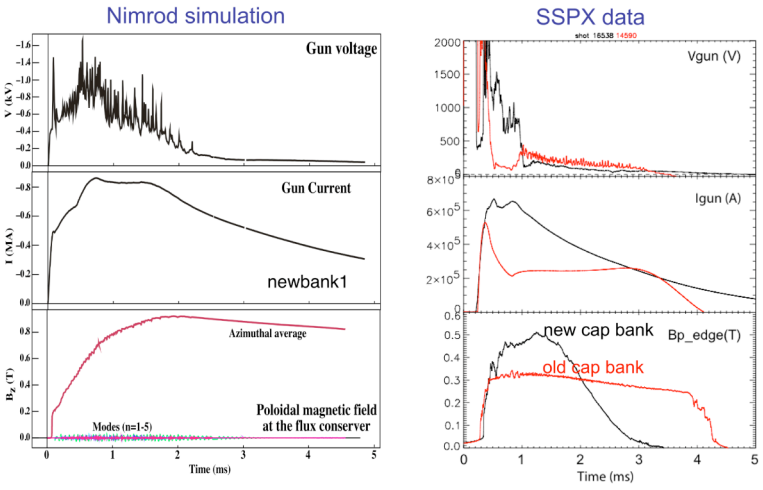
Nimrod simulation
Gun voltage
V (kV)
Gun Current
I (MA)
newbank1
Azimuthal average
Poloidal magnetic field
at the flux conserver
Modes (n=1-5)
Time (ms)
SSPX data
Vgun (V)
Igun (A)
new cap bank
Bp_edge(T)
old cap bank
Time (ms)

Fig. 1

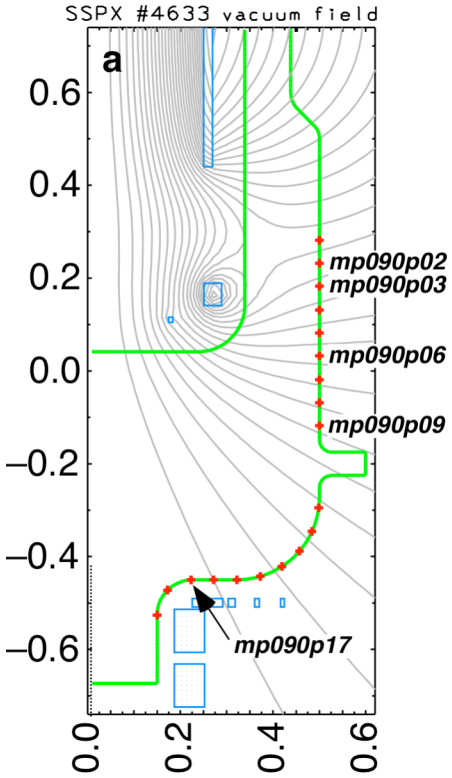
SSPX #4633 vacuum field
a
0.6
0.4
0.2
0.0
–0.2
–0.4
–0.6
0.0
0.2
0.4
0.6
mp090p02
mp090p03
mp090p06
mp090p09
mp090p17

Figure 2a

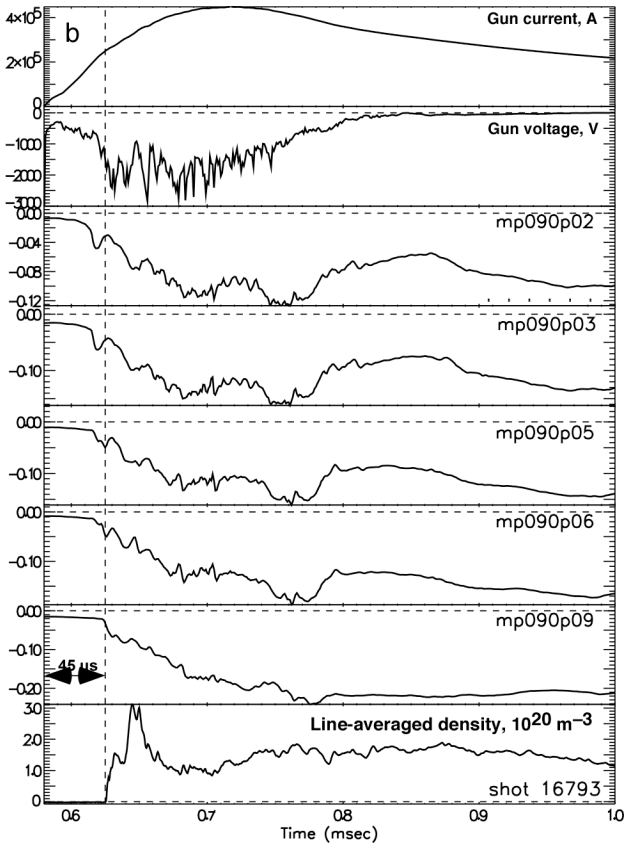
b
Gun current, A
Gun voltage, V
mp090p02
mp090p03
mp090p05
mp090p06
mp090p09
45 μs
Line-averaged density, 10^20 m^-3
shot 16793
Time (msec)

Figure 2b

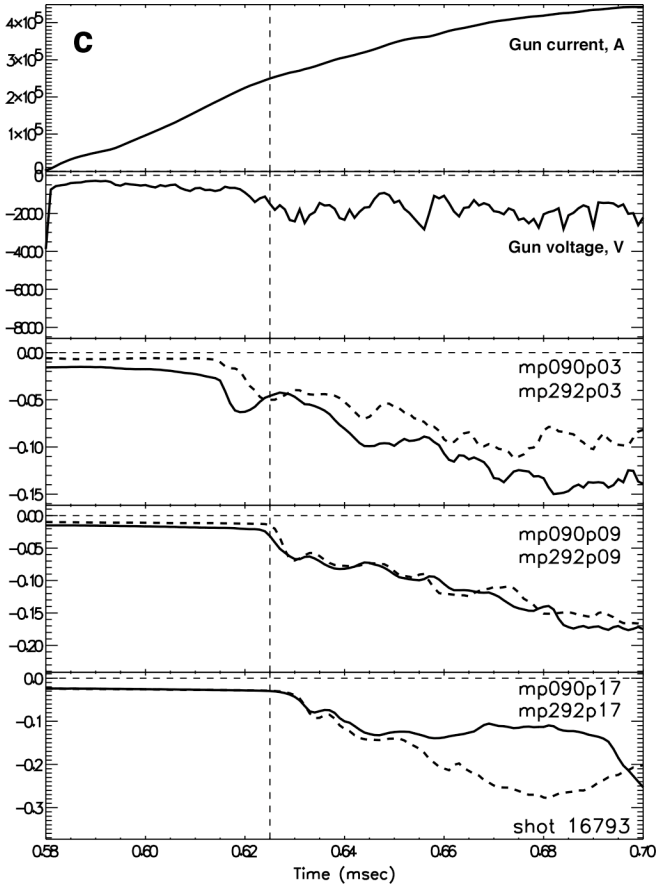
c
Gun current, A
Gun voltage, V
mp090p03
mp292p03
mp090p09
mp292p09
mp090p17
mp292p17
shot 16793
Time (msec)

Figure 2c

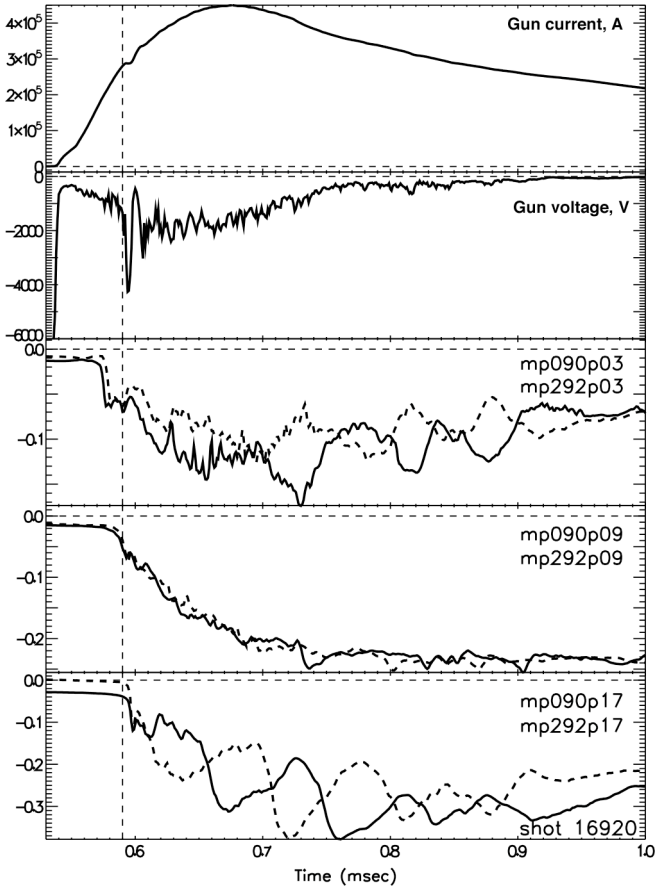
Gun current, A
Gun voltage, V
mp090p03
mp292p03
mp090p09
mp292p09
mp090p17
mp292p17
shot 16920
Time (msec)

Figure 3

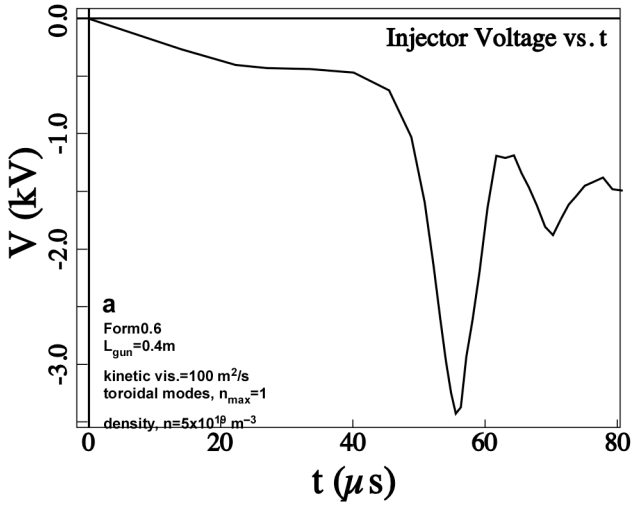

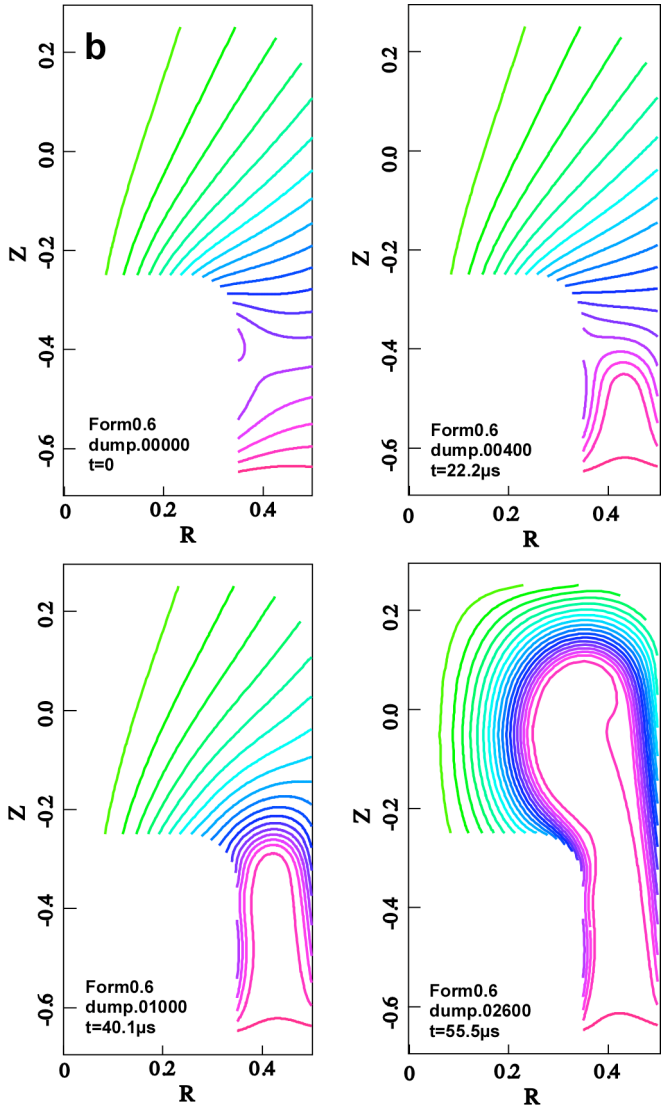

Figure 4a and b

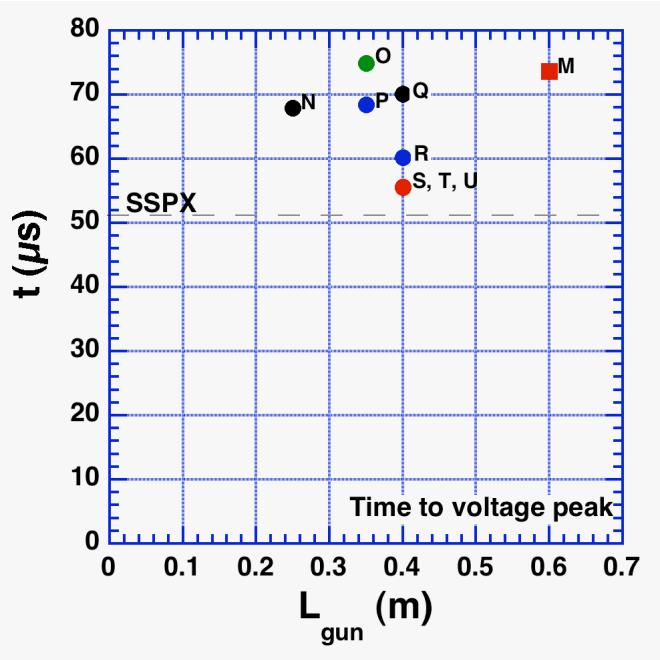
80
70
60
50
40
30
20
10
0
t (μs)
O
M
Q
N
P
R
S, T, U
SSPX
Time to voltage peak
0
0.1
0.2
0.3
0.4
0.5
0.6
0.7
L gun (m)

Figure 5

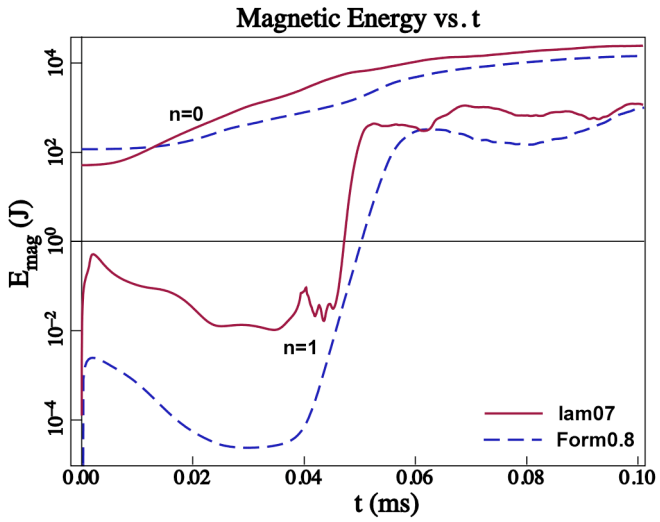
Magnetic Energy vs. t
E_{mag} (J)
10^4
10^2
10^0
10^{-2}
10^{-4}
n=0
n=1
lam07
Form0.8
0.00
0.02
0.04
0.06
0.08
0.10
t (ms)

Figure 6

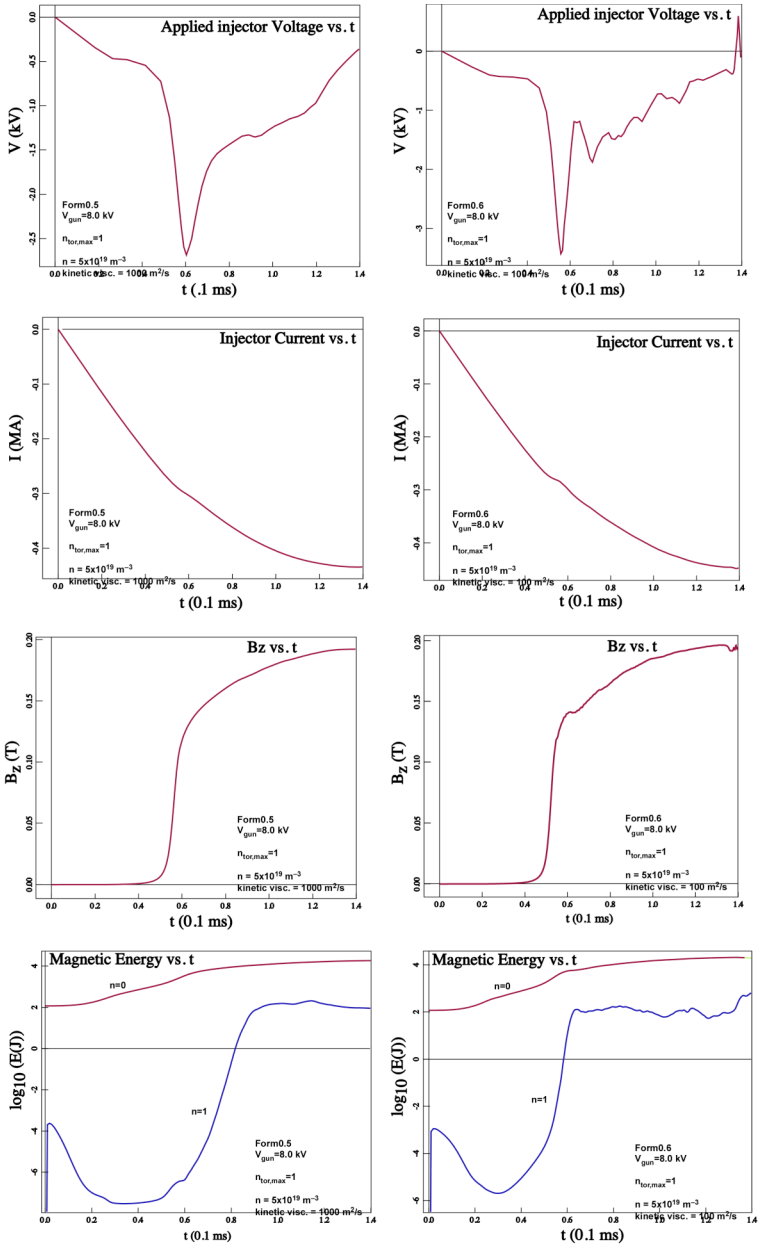
Applied injector Voltage vs. t
V (kV)
t (.1 ms)
Form0.5
V_{gun}=8.0 kV
$n_{tor,max}$=1
n = 5x10^{19} m^{-3}
kinetic visc. = 1000 m^2/s
Applied injector Voltage vs. t
V (kV)
t (0.1 ms)
Form0.6
V_{gun}=8.0 kV
$n_{tor,max}$=1
n = 5x10^{19} m^{-3}
kinetic visc. = 100 m^2/s
Injector Current vs. t
I (MA)
t (0.1 ms)
Form0.5
V_{gun}=8.0 kV
$n_{tor,max}$=1
n = 5x10^{19} m^{-3}
kinetic visc. = 1000 m^2/s
Injector Current vs. t
I (MA)
t (0.1 ms)
Form0.6
V_{gun}=8.0 kV
$n_{tor,max}$=1
n = 5x10^{19} m^{-3}
kinetic visc. = 100 m^2/s
Bz vs. t
B_Z (T)
t (0.1 ms)
Form0.5
V_{gun}=8.0 kV
$n_{tor,max}$=1
n = 5x10^{19} m^{-3}
kinetic visc. = 1000 m^2/s
Bz vs. t
B_Z (T)
t (0.1 ms)
Form0.6
V_{gun}=8.0 kV
$n_{tor,max}$=1
n = 5x10^{19} m^{-3}
kinetic visc. = 100 m^2/s
Magnetic Energy vs. t
log$_{10}$ (E(J))
n=0
n=1
t (0.1 ms)
Form0.5
V_{gun}=8.0 kV
$n_{tor,max}$=1
n = 5x10^{19} m^{-3}
kinetic visc. = 1000 m^2/s
Magnetic Energy vs. t
log$_{10}$ (E(J))
n=0
n=1
t (0.1 ms)
Form0.6
V_{gun}=8.0 kV
$n_{tor,max}$=1
n = 5x10^{19} m^{-3}
kinetic visc. = 100 m^2/s

Figure 7

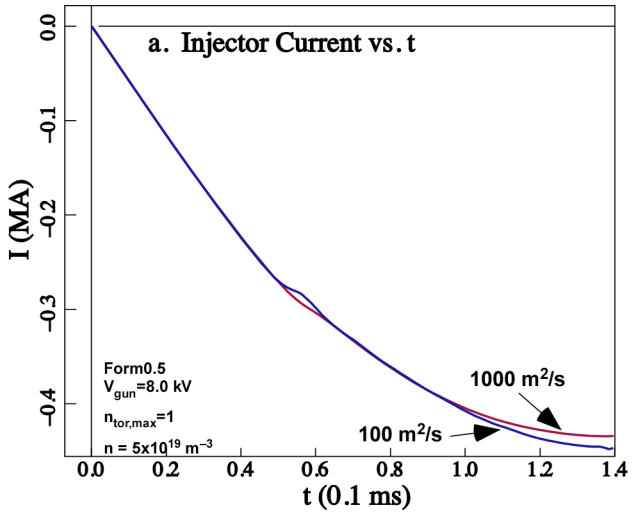

Figure 8a

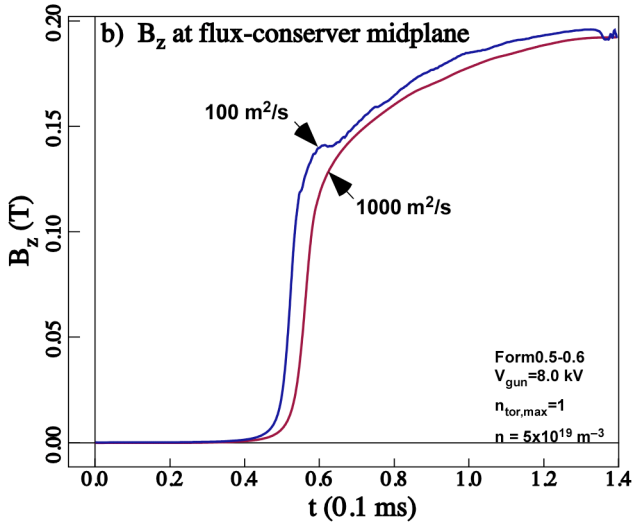

Figure 8b

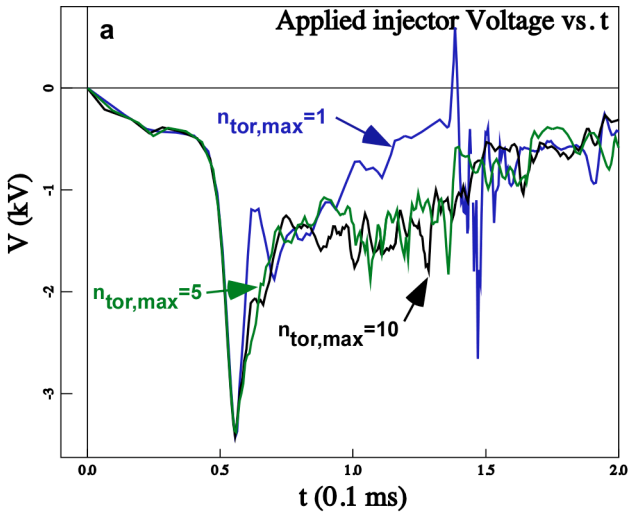

Figure 9a

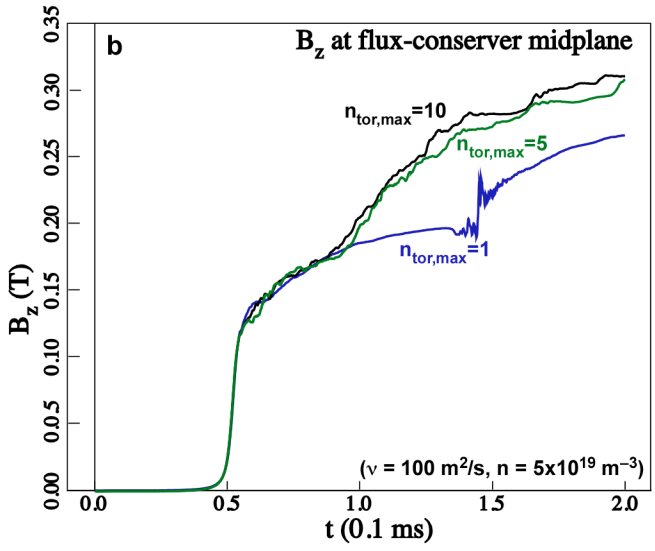

Figure 9b

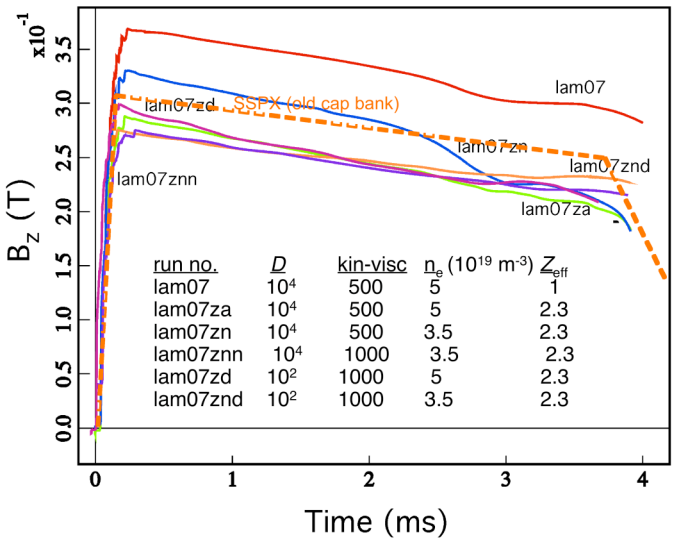

run no.	D	kin-visc	n_e (10^{19} m^{-3})	Z_{eff}
lam07	10^4	500	5	1
lam07za	10^4	500	5	2.3
lam07zn	10^4	500	3.5	2.3
lam07znn	10^4	1000	3.5	2.3
lam07zd	10^2	1000	5	2.3
lam07znd	10^2	1000	3.5	2.3

Fig. 10

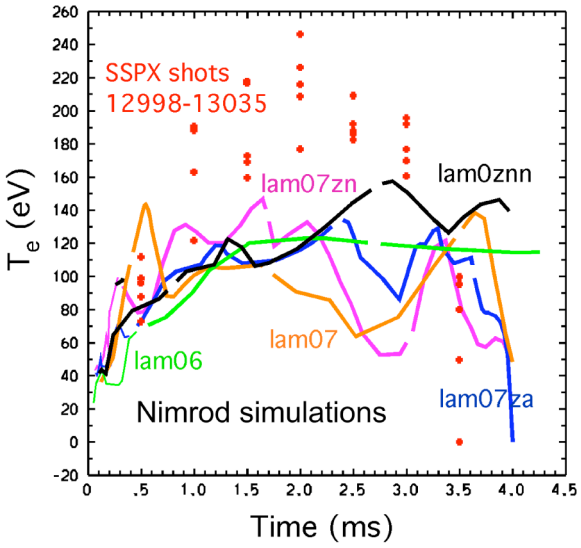

NIMROD run no.	Z_{eff}	kin-visc	n_e (10^{19} m^{-3})
lam06	1	1000	5
lam07	1	500	5
lam07za	2.3	500	5
lam07zn	2.3	500	3.5
lam07znn	2.3	1000	3.5

Fig. 11

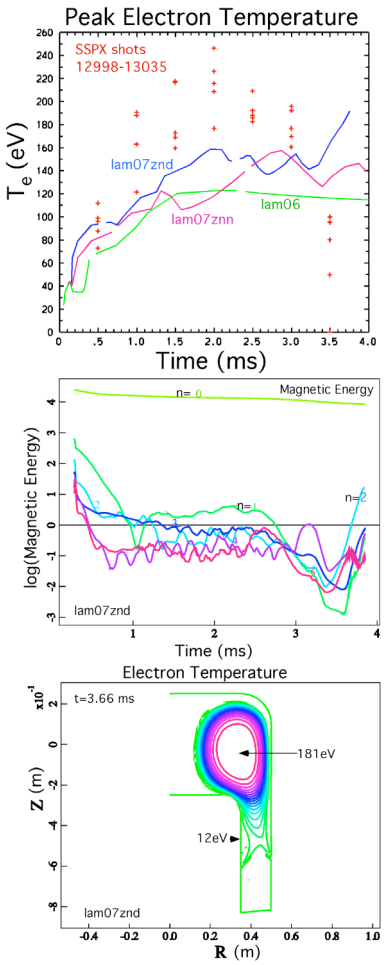
Peak Electron Temperature
SSPX shots
12998-13035
lam07znd
lam07znn
lam06
T_e (eV)
Time (ms)
Magnetic Energy
n= 0
n=1
n=2
log(Magnetic Energy)
lam07znd
Time (ms)
Electron Temperature
t=3.66 ms
181eV
12eV
lam07znd
Z (m)
R (m)

Fig. 12

Fig. 13

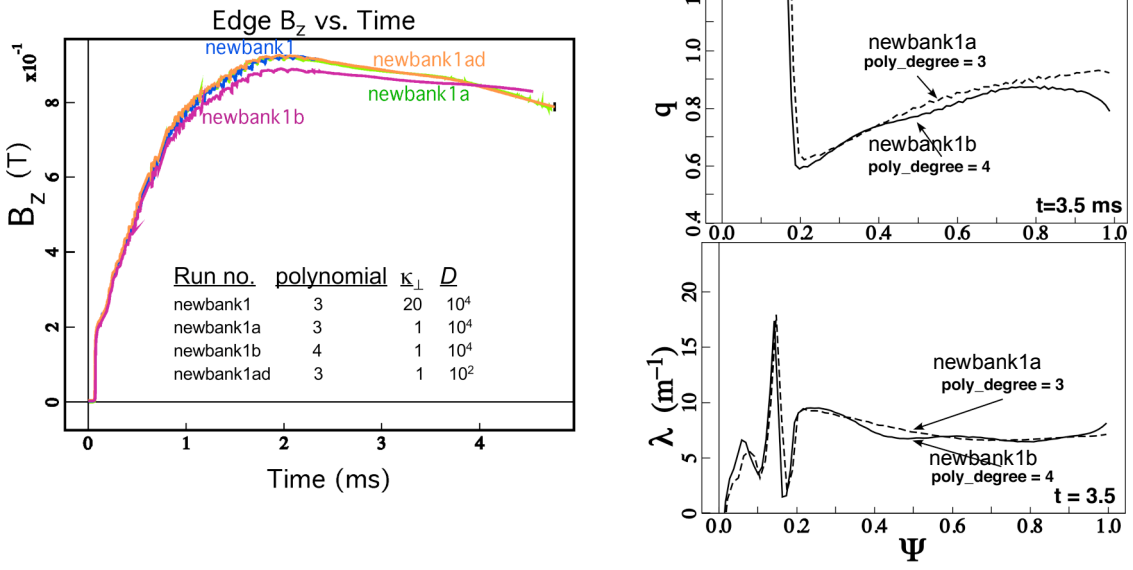

Fig. 14

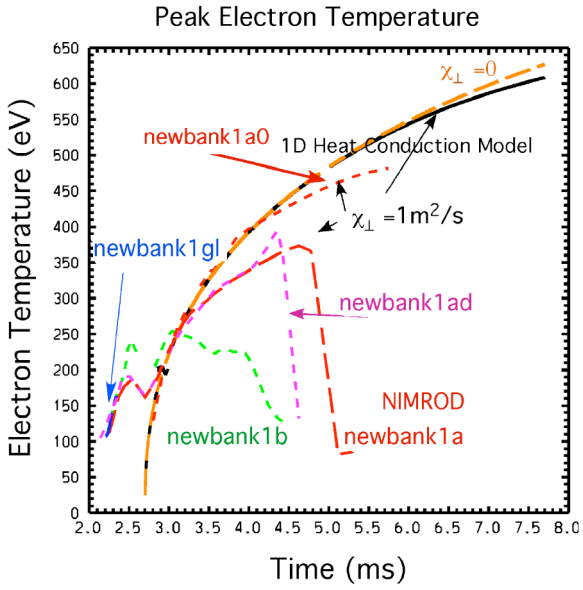

Run no.	polynomial	$\kappa_\perp$	D
newbank1a0	3 (unif), n=0	1	10^4
newbank1a	3 (unif)	1	10^4
newbank1ad	3 (unif)	1	10^2
newbank1b	4 (unif)	1	10^4
newbank1gl	4 (Gauss-Leg)	1	10^4

Fig. 15

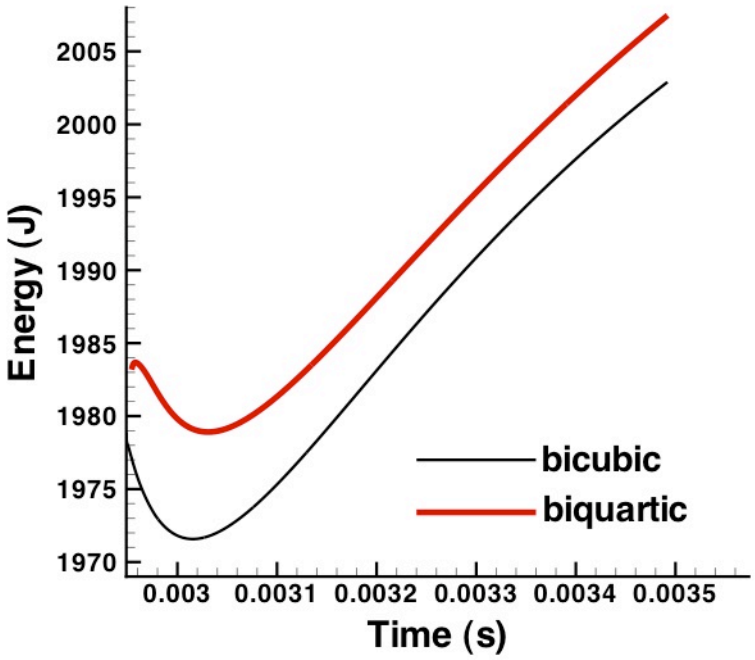
2005
2000
1995
1990
1985
1980
1975
1970
Energy (J)
0.003
0.0031
0.0032
0.0033
0.0034
0.0035
Time (s)
bicubic
biquartic

Fig. 16

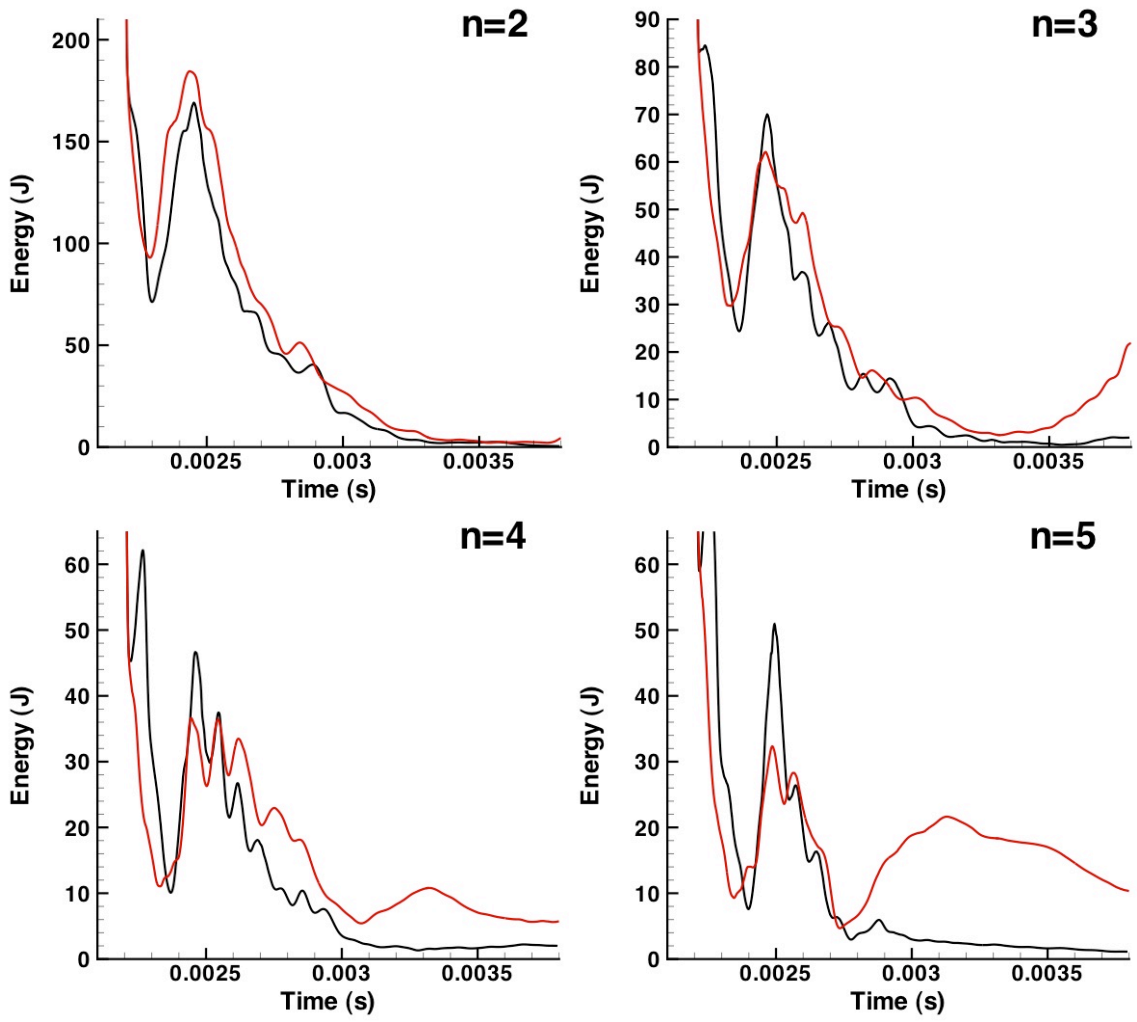

Fig. 17

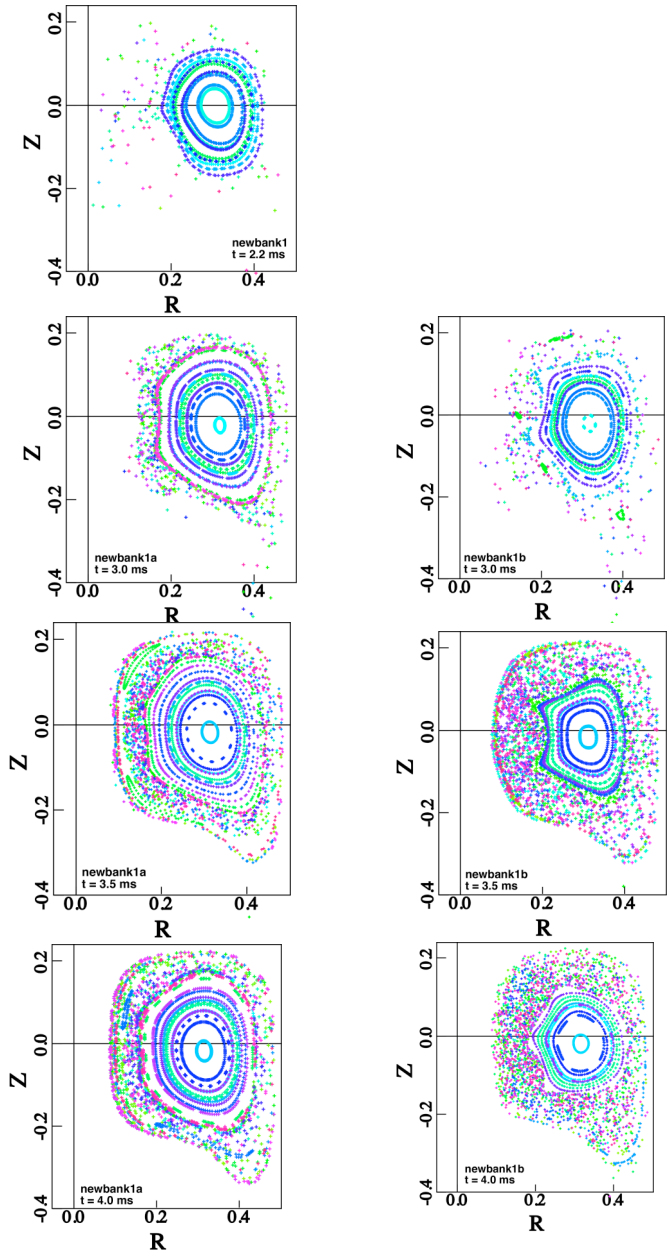
newbank1
t = 2.2 ms
newbank1a
t = 3.0 ms
newbank1b
t = 3.0 ms
newbank1a
t = 3.5 ms
newbank1b
t = 3.5 ms
newbank1a
t = 4.0 ms
newbank1b
t = 4.0 ms
Z
R
0.2
0.0
-0.2
-0.4
0.0
0.2
0.4

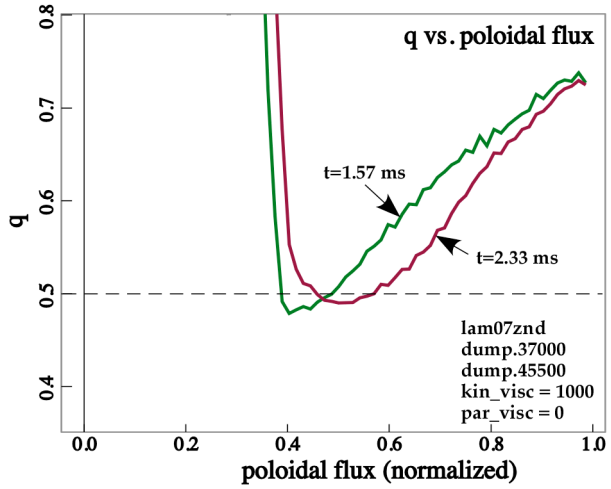
q vs. poloidal flux
t=1.57 ms
t=2.33 ms
lam07znd
dump.37000
dump.45500
kin_visc = 1000
par_visc = 0
q
poloidal flux (normalized)

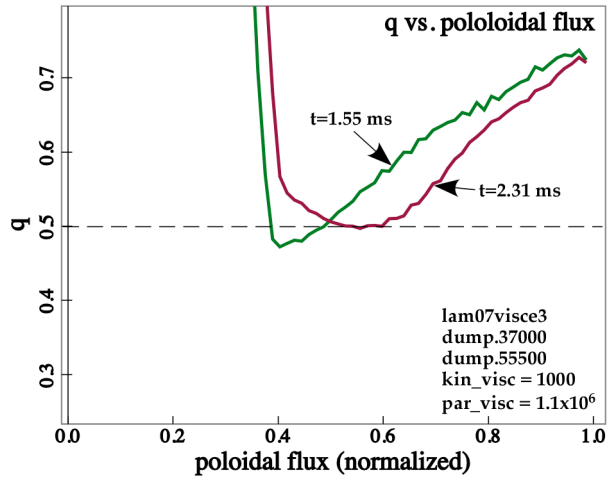
q vs. pololoidal flux
t=1.55 ms
t=2.31 ms
lam07visce3
dump.37000
dump.55500
kin_visc = 1000
par_visc = 1.1x10^6
q
poloidal flux (normalized)

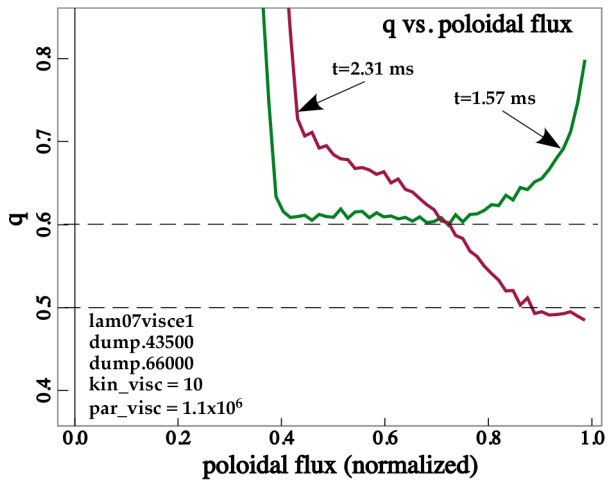
q vs. poloidal flux
t=2.31 ms
t=1.57 ms
lam07visce1
dump.43500
dump.66000
kin_visc = 10
par_visc = 1.1x10^6
q
poloidal flux (normalized)

Fig. 18

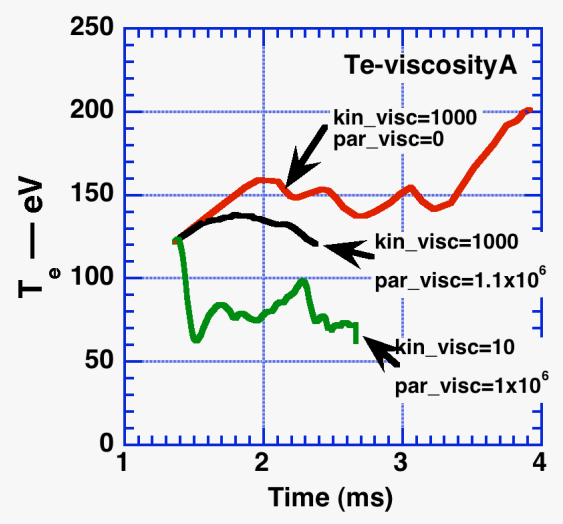
Te-viscosityA
kin_visc=1000
par_visc=0
kin_visc=1000
par_visc=1.1x10^6
kin_visc=10
par_visc=1x10^6
T_e — eV
Time (ms)
250
200
150
100
50
0
1
2
3
4

Fig. 19

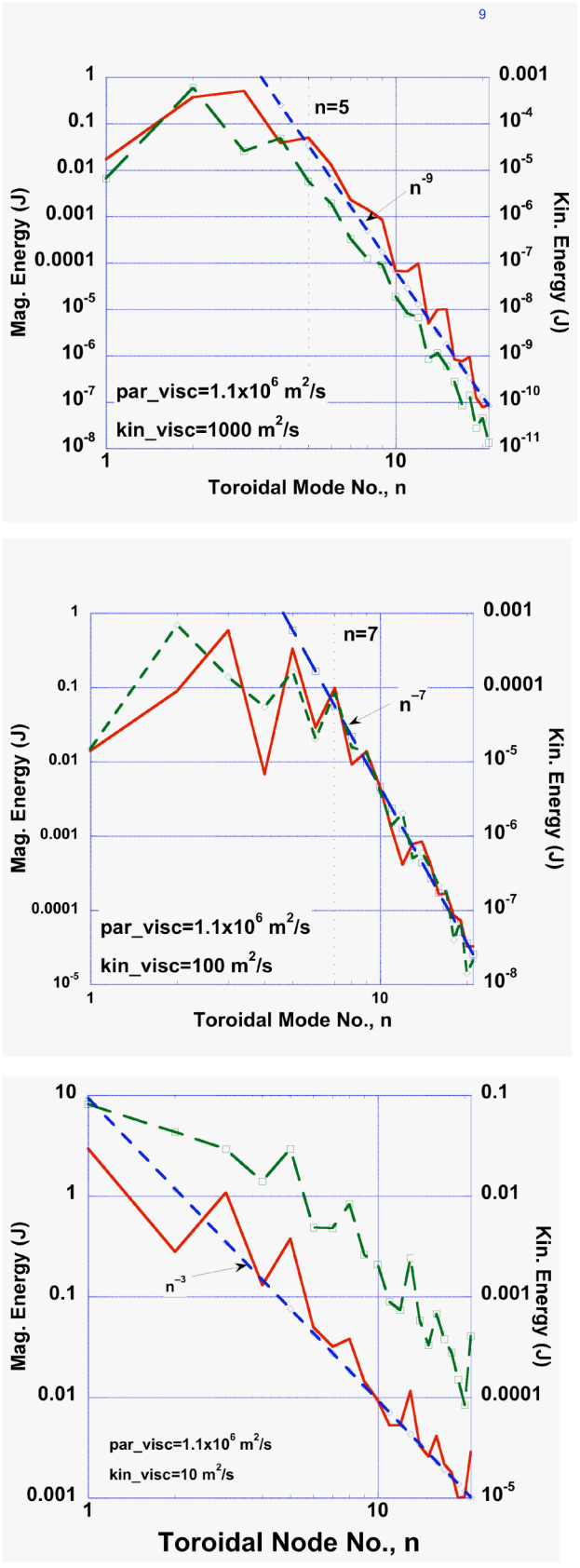
n=5
n^-9
par_visc=1.1x10^6 m^2/s
kin_visc=1000 m^2/s
Mag. Energy (J)
Kin. Energy (J)
Toroidal Mode No., n
n=7
n^-7
par_visc=1.1x10^6 m^2/s
kin_visc=100 m^2/s
Mag. Energy (J)
Kin. Energy (J)
Toroidal Mode No., n
n^-3
par_visc=1.1x10^6 m^2/s
kin_visc=10 m^2/s
Mag. Energy (J)
Kin. Energy (J)
Toroidal Node No., n

Fig. 20